HAL
open science

Generalized Pareto processes for simulating space-time extreme events

Fátima Palacios-Rodríguez, Gwladys Toulemonde, Julie Carreau, Thomas Opitz

To cite this version:

Fátima Palacios-Rodríguez, Gwladys Toulemonde, Julie Carreau, Thomas Opitz. Generalized Pareto processes for simulating space-time extreme events. 2019. hal-02136681v1

HAL Id: hal-02136681

https://hal.science/hal-02136681v1

Preprint submitted on 19 Jun 2019 (v1), last revised 7 Oct 2020 (v3)

HAL is a multi-disciplinary open access archive for the deposit and dissemination of scientific research documents, whether they are published or not. The documents may come from teaching and research institutions in France or abroad, or from public or private research centers.

L'archive ouverte pluridisciplinaire **HAL**, est destinée au dépôt et à la diffusion de documents scientifiques de niveau recherche, publiés ou non, émanant des établissements d'enseignement et de recherche français ou étrangers, des laboratoires publics ou privés.

Generalized Pareto processes for simulating space-time extreme events

F. Palacios-Rodríguez (corresponding author)

Inria Project-team LEMON. IMAG, Université de Montpellier. CNRS. Montpellier. France.

E-mail: fatima.palacios-rodriguez@inria.fr

G. Toulemonde

IMAG, Université de Montpellier. CNRS. Inria, Project-team LEMON. Montpellier. France.

J. Carreau

HydroSciences Montpellier, CNRS/IRD, Université de Montpellier. Montpellier. France.

T. Opitz

Biostatistics and Spatial Processes, INRA Avignon. France.

Summary. To better manage the risks of destructive natural disasters, impact models can be fed with simulations of extreme scenarios to study sensitivity to temporal and spatial variability. We propose semi-parametric stochastic simulation of realistic spatio-temporal extreme fields using a moderate number of observed extreme space-time episodes to generate an unlimited number of extreme scenarios of any magnitude. Our framework draws sound theoretical justification from extreme value theory, building on generalized Pareto limit processes. For illustration on hourly gridded precipitation data in Mediterranean France, we calculate risk measures using extreme event simulations for yet unobserved magnitudes.

Keywords: extreme-value theory; precipitation; space-time Pareto processes; stochastic simulation.

1. Introduction

Extreme events of geophysical processes such as precipitation extend over space and time, and they can entail devastating consequences for human societies and ecosystems. Flash floods in southern France constitute highly destructive natural phenomena causing material damage and threatening the human lives (Vinet et al., 2016). Since damage and costs of floods have been increasing over the last decades, the understanding of temporal and spatial variability of rainfall

patterns generating such floods receives considerable attention from the authorities (European Environment Agency, 2007). To help with this understanding, we here develop a stochastic simulation method of realistic spatio-temporal extreme scenarios, which can be fed to impact models.

Extreme-value theory (EVT) for spatial data proposes data-based stochastic modeling of such extreme events for predicting probabilities, risks and uncertainty behavior (Coles, 2001; de Haan and Ferreira, 2006; Ferreira and de Haan, 2014). Due to very complex deterministic and probabilistic patterns in such processes and the high dimension of data sets, realistic spatio-temporal modeling is challenging. In this work, we instead develop a data-driven non-parametric approach to handle extremal space-time dependence by transforming observed marginal quantiles in a spatially and temporally coherent way. We illustrate our method on a high-dimensional data set of gridded hourly reanalysis data. Our procedure draws sound justification from asymptotic theory for threshold exceedances with a strong probabilistic interpretation. We will explain how it allows us to flexibly define extreme episodes in space-time data based on different ways of aggregating marginal return periods over space and time.

Block-maxima and peaks-over-threshold (POT) methods are two widely known strategies in univariate EVT to identify extreme events in a data set. While the block-maxima method is based on the division of the observation period into non-overlapping periods of equal size (for instance months or years) to extract the maximum observation in each period (Ferreira and de Haan, 2015), the POT method consists in the study of positive exceedances above a given high threshold (Pickands III, 1975; Embrechts et al., 1997; Beirlant et al., 2004). Max-stable processes, introduced by de Haan (1984), are the natural infinite-dimensional generalization of the univariate generalized extreme value (GEV) distribution, which constitutes the only limiting distribution in block-maxima approach. Ferreira and de Haan (2014) and Dombry and Ribatet (2015) showed that generalized Pareto (GP) processes are the only possible asymptotic limits for threshold exceedances. Both approaches are closely linked through theoretical tail stability properties.

Several approaches were developed for stochastic simulation of spatial max-stable fields (Dombry et al. (2013, 2016); Oesting et al. (2018b,a)). Since max-stable processes are linked to the block-maxima approach, their realizations aggregate information of several of the underlying original events which may limit the physical interpretations of the simulated processes. Consequently, these simulations appear to be more appropriate for studying long-term events such as the erosion of the coastline (Chailan et al., 2017).

On the other hand, GP processes represent the original events that fulfill a threshold exceedance condition. They can be represented constructively by multiplying a random scaling variable with a so-called spectral process, the latter characterizing the spatial variation in the extreme events (Ferreira and de Haan (2014); Dombry and Ribatet (2015); Thibaud and Opitz (2015)). In practice, one usually first fits a parametric model for the spectral processes, and the estimators are then plugged in for simulation. In contrast, we here develop an algorithm for extracting observed spectral processes from data, and we then combine them with newly sampled scaling variables to generate new realizations of the extreme events.

Since extreme events are frequently spatio-temporal in nature, their duration has to be accounted for. A semi-parametric method to simulate extreme spatio-temporal fields of wave heights in the Gulf of Lion (France) was proposed in Chailan et al. (2017) based on methods for the spatial setting developed by Caires et al. (2011) and Ferreira and de Haan (2014). The approach proposed in our work is motivated by Chailan et al. (2017) and provides three major novelties. Firstly, our procedure allows for an infinite number of simulations. Secondly, we embed our semiparametric resampling idea in the framework of GP processes, which allows for a clear probabilistic interpretation of extreme events. Thirdly, a flexible general procedure is presented to identify extreme events and quantify their magnitude by accounting for space-time aggregation through homogeneous cost functionals that encapsulate operations such as averaging or taking maxima.

The paper is structured as follows. Section 2 presents theory for space-time GP processes. Techniques to practically implement and validate the spatio-temporal GP framework are proposed in Section 3. Our algorithm to generate extreme space-time scenarios is developed in Section 4. We illustrate our approach on hourly rainfall reanalysis data available on a 1 km^2 grid in Southern France over a 10-year period from 1997 to 2007 in Section 5. In this case study, we perform a comparative analysis based on two conventional risk measures using simulated extreme scenarios. Conclusions and future research are given in Section 6.

2. Theory of space-time GP processes

We write $\mathcal{S}$ for a compact subset of $\mathbb{R}^d$ to denote the area of interest and $\mathcal{T}$ for a compact subset of $\mathbb{R}^+$ to denote the time dimension, and we denote by $C(\mathcal{S}\times\mathcal{T})$ the space of continuous functions on $\mathcal{S} \times \mathcal{T}$, equipped with the supremum norm. The restriction of $C(\mathcal{S} \times \mathcal{T})$ to non-negative functions is written $C_+(\mathcal{S} \times \mathcal{T})$.

In multivariate EVT, a GP limit was introduced in Rootzén and Tajvidi (2006) by condition-

ing on an exceedance event in at least one component. The aforementioned idea was extended to infinite-dimensional spaces by the definition of GP process in Ferreira and de Haan (2014) where the condition is based on exceedances of the supremum over space. To gain flexibility in the definition of the conditioning extreme events, Dombry and Ribatet (2015) provided the notion of ℓ-Pareto processes by considering more general exceedances defined in terms of a homogeneous cost functional denoted ℓ. Our focus here is on the spatial and temporal dimensions for the extent of extreme events. Since we aim to model phenomena that exceed a certain extreme threshold, we start by defining and characterizing space-time generalized ℓ-Pareto processes. The following constructive definition generalizes Dombry and Ribatet (2015).

2.1. Construction of space-time GP processes

We define a *cost functional* $\ell : C_+(\mathcal{S} \times \mathcal{T}) \to [0, +\infty)$ as a continuous nonnegative function that is homogeneous, i.e. $\ell(tf) = t\ell(f)$ for $t \geq 0$. Examples of such ℓ are the functions of maximum, minimum, average, or the value at a specific point $(s_0, t_0) \in \mathcal{S} \times \mathcal{T}$.

Definition 1 (Standard space-time ℓ-Pareto process). *Let $W^* = \{W^*(s,t)\}_{s\in\mathcal{S},t\in\mathcal{T}}$ be a stochactic process in $C_+(\mathcal{S} \times \mathcal{T})$. We call W^* a* standard space-time ℓ-Pareto process *if it can be represented as*

$$W^*(s,t) \stackrel{d}{=} RY(s,t) \tag{1}$$

where

(a) Y is a stochastic process in $C_+(\mathcal{S} \times \mathcal{T})$ satisfying $\ell(Y) = 1$;
(b) R has Pareto distribution with scale 1 and shape γ, i.e., $\mathbb{P}(R > r) = r^{-\gamma}$, $r > 1$;
(c) Y and R are stochastically independent.

The above definition is equivalent to the POT stability: for any $u \geq 1$, the distribution of the renormalized threshold-exceeding process $\{u^{-1}W^*|\ell(W^*) \geq u\}$ is equal to the distribution of W^*; see Theorem 2 of Dombry and Ribatet (2015). By construction, we get $Y \stackrel{d}{=} W^*/\ell(W^*)$ and $R \stackrel{d}{=} \ell(W^*)$. A generalized version of such Pareto processes is given in the following Definition 2 by allowing for flexibility in the marginal distributions according to the location-scale-shape parametrization commonly used in univariate EVT.

Definition 2 (Generalized space-time ℓ-Pareto process). *Given an ℓ-Pareto process $W^*(s,t)$ constructed according to Definition 1 and continuous real functions $\sigma(s,t) > 0$, $\mu(s,t)$*

and $\gamma(s,t)$ *in* $C(\mathcal{S}\times\mathcal{T})$*, a* generalized space-time ℓ-Pareto process *is any process constructed as*

$$W(s,t) \stackrel{d}{=} \begin{cases} \mu(s,t)+\sigma(s,t)\{W^*(s,t)^{\gamma(s,t)}-1\}/\gamma(s,t), & \gamma(s,t)\neq 0, \\ \mu(s,t)+\sigma(s,t)\log W^*(s,t), & \gamma(s,t)=0. \end{cases} \tag{2}$$

2.2. Limits for space-time GP processes

We shortly recall the two main limits for characterizing extremes of stochastic processes: max-stable processes and Pareto processes; we refer the reader to the literature for technical details (Lin and de Haan, 2001; de Haan and Ferreira, 2006; Ferreira and de Haan, 2014; Thibaud and Opitz, 2015; Dombry and Ribatet, 2015). We use the symbol "$\Rightarrow$" to represent variants of weak convergence of random elements from the univariate, multivariate or functional domain.

Consider independent copies $X_1,\ldots,X_n$ of a stochastic space-time process $X=\{X(s,t)\}_{s\in\mathcal{S},t\in\mathcal{T}}$ with continuous trajectories. We say that the process X is in the functional maximum domain of attraction of a max-stable process $Z=\{Z(s,t)\}_{s\in\mathcal{S},t\in\mathcal{T}}$ with continuous trajectories if there exist continuous functions $a_n>0$ and b_n such that

$$\left\{\max_{1\le i\le n}\frac{X_i(s,t)-b_n(s,t)}{a_n(s,t)}\right\}_{s\in\mathcal{S},t\in\mathcal{T}} \Rightarrow \{Z(s,t)\}_{s\in\mathcal{S},t\in\mathcal{T}}\,. \tag{3}$$

Further details about space-time max-stable processes can be found in Davis et al. (2013a,b).

The convergence of the dependence structure and of marginal distributions in (3) can be studied separately; see de Haan and Ferreira (2006, Section 9.2). A standardised process $X^*=X^*(s,t)$ can be defined as $X^*(s,t)=1/(1-F_{(s,t)}(X(s,t)))$, $s\in\mathcal{S}$, $t\in\mathcal{T}$, where $F_{(s,t)}$ denotes the distribution of $X(s,t)$. Equivalently, if H denotes the distribution function of a standard Pareto distribution, we apply the transformation $X^*(s,t)=H^{-1}(F_{(s,t)}(X(s,t)))$. If X has continuous marginal distributions $F_{(s,t)}$, then X^* has marginal standard Pareto distributions. For $a_n\equiv n$, $b_n\equiv 0$, the max-stable limit for X^* in (3) is a standard max-stable process $Z^*=\{Z^*(s,t)\}_{s\in\mathcal{S},t\in\mathcal{T}}$ with unit Fréchet marginal distributions; see de Haan and Ferreira (2006, Definition 9.2.4).

If X^* is in the maximum domain of attraction of a max-stable process Z^* and the cost functional ℓ is continuous at 0, we get the convergence of ℓ-*exceedances* on the standard scale:

$$\left\{u^{-1}X^*(s,t)|\ell(X^*(s,t))>u\right\}\Rightarrow\{W^*(s,t)\}\,,\ u\to\infty, \tag{4}$$

where $W^*(s,t)$ is a standard space-time ℓ-Pareto process as in Definition 1 (Dombry and Ribatet, 2015, Theorem 3). Conversely, if the convergence in (4) holds for ℓ chosen as the maximum norm, then convergence in (3) of the max-stable process X^* to Z^* follows. An example of

Pareto processes with log-Gaussian profile process is given in Section 1 in the supplementary material.

3. Practice of space-time GP processes

In practice, we use the limit theory exposed in Section 2 for conducting statistical analyses on extreme events based on finite-sample data, which poses a number of practical challenges. In this section, we propose solutions for three issues : the standardization of marginal distributions (Section 3.1), the definition of extreme space-time episodes (Section 3.2), the analysis and verification of asymptotic stability properties (so-called *threshold-stability*, see Section 3.3).

3.1. Marginal transformations

We first discuss suitable marginal transformations of X such that X^* satisfies convergence with respect to ℓ-exceedances in (4). In theory, values of $X^*(s,t)$ close to 0 are pushed to 0 when $u \to \infty$ in (4), but in practice the use of a high but finite threshold u leads to non-zero values in $u^{-1}X^*(s,t)$. Therefore, a certain ambiguity persists in practice to define the standardization for relatively small, non extreme values of $X(s,t)$. In particular, if the minimum value of the data process X arises with positive and non negligible probability, such as the value 0 for the absence of precipitation in our application study, then this minimum value should be mapped to 0 in the standardized process X^*. Here, we develop the general idea of such transformations and a more specific transformation for precipitation data is proposed in Section 5. We choose a distribution G whose survival function $\bar{G}$ verifies: $x\,\bar{G}(x) \to 1,\ x \to \infty$, and $\bar{G}(0) = 1$; we write $G^{\leftarrow}$ for the (generalized) inverse function of G. We then define the transformation $T = T_{s,t}$ towards the standardized process X^* as follows:

$$X^*(s,t) = T(X(s,t)) = G^{\leftarrow}(F_{(s,t)}(X(s,t))) \tag{5}$$

where $F_{(s,t)}$ denotes the distribution of $X(s,t)$. The (generalized) inverse transformation of T can be defined as $T^{\leftarrow}(f) = F^{\leftarrow}_{(s,t)}(G(f))$ for $f \in C_+(\mathcal{S} \times \mathcal{T})$, with $F^{\leftarrow}_{(s,t)}$ the (generalized) inverse function of $F_{(s,t)}$.

Regarding marginal modeling, it is natural to use a tail representation motivated by univariate EVT, whose parametrization corresponds directly to the GP process in Definition 2. For a fixed high threshold function $u(s,t)$, we assume that

$$\mathbb{P}(X(s,t) > x) = 1 - F_{(s,t)}(x) = \left[1 + \gamma(s,t)\frac{x - \mu(s,t)}{\sigma(s,t)}\right]_+^{-1/\gamma(s,t)} \tag{6}$$

for $x > u(s,t)$, with parameter functions for position $\mu(s,t) < u(s,t)$, for scale $\sigma(s,t) > 0$ and for shape $\gamma(s,t)$, such that the right-hand side of (6) is less than 1 (Thibaud and Opitz, 2015). For data values $X(s,t)$ below $u(s,t)$, we may use appropriately chosen empirical distribution functions or any other useful model, where the probability mass below $u(s,t)$ should amount to $F_{(s,t)}(u(s,t))$ with $F_{(s,t)}$ defined in (6).

The standardization in (5) leads to $\mathbb{P}(T(X(s,t)) > T(x)) \sim \frac{1}{T(x)}$ for large x, and therefore to $\mathbb{P}(T(X'(s,t)) > T(X(s,t)) \mid X(s,t) = x(s,t)) \sim \frac{1}{T(x(s,t))}$ for an independent copy X' of X. The observed value of $T(X(s,t))$ can be interpreted as the (marginal) return period of the observation $X(s,t)$, and at high quantiles we can interpret X^* as the space-time process of marginal return periods. The cost functional ℓ (approximately) aggregates marginal return periods $X^*(s,t)$ into return periods $\ell(X^*)$ for space-time episodes. For details about the definition of return periods, see Section 2 in the supplementary material.

3.2. Defining extreme episodes

For the purpose of simulating realistic spatio-temporal extreme scenarios, we have to define what "extreme" means. With environmental data, we often have only a single observation of the space-time process X, and very high values typically tend cluster temporally within relatively short sub-periods. We consider such sub-periods as extreme space-time events. If it is realistic to assume that temporal dependence of extremes becomes negligible for relatively large time lags, theoretical results based on independent processes as in Section 2 can be used. In the space-time GP process framework, the value of ℓ quantifies the magnitude of events. In practice, we apply ℓ to a large collection of candidate episodes to extract the most extreme ones. Our extraction algorithm is designed to avoid temporal intersection of the selected extreme episodes.

There is no unique definition of an extreme event, i.e. of the cost functional ℓ, rather it depends on the nature of the considered phenomenon, on the data set, on the objective of the study, and also on the structure of the model (McPhillips et al., 2018). Expert knowledge may suggest how to measure the extreme nature of an event, where the question of how to combine criteria related to duration, spatial extent and magnitude is recurrent. For instance, French et al. (2018) develop new visualizations of extreme heat waves by composing a temporal and spatial cost functional. Chailan et al. (2017) extract extreme wave heights based on spatio-temporal maxima in sliding time windows.

In the following, we use the idea of sliding space-time windows and specify the support of the cost functional ℓ introduced in Section 2.1 as a *neighborhood* $\mathcal{N}(s,t)$ indexed by $s \in \mathcal{S}$ and $t \in \mathcal{T}$.

In practice, the window size defines the maximal time duration and spatial extent of extreme events. The space index s may be missing if we consider the full study area for extracting extreme events. This neighborhood could be defined through an event duration δ in time, and the spatial support could be the full study area or a sub-region such as a catchment or a certain distance buffer around a specific site s_0. To indicate the local support of the cost functional defined as a neighborhood around (s,t), we use the notation $\ell_{s,t}(X^*) = \ell(\{X^*(s',t'),\ (s',t') \in \mathcal{N}(s,t)\})$.

We propose to define $\mathcal{N}(s,t)$ as the product of a spatial neighborhood $\mathcal{N}(s)$ (e.g., $\{s' \in \mathcal{S} \mid \|s-s'\| \leq 15km\}$) and a temporal neighborhood $\mathcal{N}(t)$ (e.g.m, $\{t' \in \mathcal{T} \mid |t-t'| \leq 6\text{hours}\}$), $\mathcal{N}(s,t) = \mathcal{N}(s) \times \mathcal{N}(t)$. Useful cost functionals ℓ for space-time episodes are obtained by composing spatial functional ℓ^S with a temporal functional ℓ^T, the latter applied to the values of ℓ^S observed over a number of consecutive time steps:

$$\ell_{s,t}(X^*) = \ell^T(\ell^S_{s,t-\delta_1}(X^*), \ldots, \ell^S_{s,t+\delta_2}(X^*)), \tag{7}$$

with $\ell^S_{s,t}(X^*) = \ell^S(\{X^*(s',t) \mid s' \in \mathcal{N}(s)\})$ and $\delta = \delta_1 + \delta_2 + 1$. Moreover, based taking on $\ell^S_{s,t}(X^*)$ we can define cost functionals that combine the values obtained for all spatial neighborhoods $\mathcal{N}(s)$ by taking their maximum value (or again, any other spatial aggregation value. In this case, we define:

$$\ell_t(X^*) = \max_{s \in \mathcal{S}} \ell^S_{s,t}(X^*). \tag{8}$$

If X satisfies the functional domain of attraction condition (3), then

$$\mathbb{P}(\ell(X^*) > u) \sim \theta_\ell / u, \quad u \to \infty, \tag{9}$$

where θ_ℓ is the *ℓ-extremal coefficient* (see Engelke et al., 2018, for details). When $\ell_{s,t}$ is the maximum function, the ℓ-extremal coefficient $\theta_{\ell_{s,t}}$ defines the classical extremal coefficient of the domain $\mathcal{N}(s,t)$ (see example 4 of Engelke et al., 2018).

Using (9), we can calculate approximate return levels for extreme episodes characterized as ℓ-exceedances above a large threshold u. The simplest case arises for $\theta_\ell = 1$, i.e., when θ_ℓ is known beforehand and we do not have to estimate it from data. For instance, if $(s_0,t_0) \in \mathcal{S} \times \mathcal{T}$ is a fixed space-time point, we can define the cost functional value $\ell(X^*)$ as $X^*(s_0,t_0)$, and $\theta_\ell = 1$. Moreover, $\theta_\ell = 1$ if ℓ is the average, i.e. $\ell_{s,t}(x) = \frac{1}{|\mathcal{N}(s,t)|}\int_{\mathcal{N}(s,t)} x(s',t')\,\mathrm{d}(s',t')$; see Ferreira et al. (2012, Proposition 2.2). When $\theta_\ell \neq 1$, an estimator of θ_ℓ can be plugged into (9), such as a weighted least square estimator (Engelke et al., 2018). Finally, since $\mathbb{P}(\ell((X')^*) > \ell(X^*) \mid X^* = x^*) \sim \theta_\ell / \ell(x^*)$ at high quantiles of $\ell(X^*)$ for an independent copy X' of X, we can interpret $\ell(x^*)/\theta_\ell$ as the return period of an extreme event x^*.

3.3. Techniques to analyze asymptotic dependence

The functional domain of attraction condition in (3) is the theoretical basis for using GP processes. It requires that a relatively strong type of extremal dependence, known as asymptotic dependence, prevails in the data-generating process X, at least for small distances in space and time. With asymptotic dependence between two points (s,t) and $(s',t') = (s+\Delta s, t+\Delta t)$, we observe a positive limit of the probability $F_{(s',t')}(X(s',t')) > u \mid F_{(s,t)}(X(s,t)) > u$ as $u \to 1$. In this case, so-called threshold stability holds when moving towards higher quantiles, such that the typical spatial and temporal extent of clusters of extreme values does not depend on event magnitude. In practice, we should verify that data exhibit such asymptotic dependence. We shortly discuss two approaches: studying empirical extremal coefficients; and techniques for checking the independence of observed scale variable $\ell(X^*)$ and profile process $X^*/\ell(X^*)$.

3.3.1. Spatial and temporal extremal coefficient functions

Pairwise extremal coefficients provide a summary of extremal dependence with respect to distance in space and time and are calculated from bivariate data; see Section 3 in the supplementary material for details on empirical estimation. We consider first the spatial extremal coefficient function $\theta^{spa}(h)$ to measure extremal dependence between sites separated by spatial distance h at a given time, and second the temporal extremal coefficient function $\theta^{tim}(k)$ to measure extremal dependence for a time lag k at a given site. We estimate $\theta^{spa}(h)$ using observation pairs with structure $(X(s,t_i), X(s+\Delta s, t_i))$ where $\Delta s = h$, and we estimate $\theta^{tim}(k)$ from observation pairs $(\max_{s\in\mathcal{S}} X(s,t_i), \max_{s\in\mathcal{S}} X(s,t_i+k))$.

3.3.2. Independence of scale and profile

The POT stability manifests itself through the (approximate) independence between the profile process $Y = X^*/\ell(X^*)$ and the random scale $R = \ell(X^*)$ for $\ell(X^*) > u$. In practice, the threshold u should be high enough for this property to hold approximately, such that the limit process in (4) becomes a useful approximation to data. Due to the very high dimension of the profile process in the space-time setting, it is difficult to check this independence directly based on observed scales and profiles. Instead, we propose to check for the absence of strong trends in summary statistics of Y with respect to the event magnitude R, which would indicate dependence between Y and R.

In our application, we will focus on checking the scale-profile independence in space by considering the set of extreme spatial episodes W_t^* satisfying $\ell_t^S(W_t^*) > u$, and we use two

summary statistics calculated from the profile processes $Y_t = W_t^*/\ell_t(W_t^*)$. First, consider $f_{u'}(Y_t)$ defined as the proportion of sites s where $Y_t(s) \leq u'$: useful values of u' are relatively small or large quantiles of Y_t, to check for trends in the amplitude of Y_t with respect to $\ell_t(W_t^*)$. Second, consider the empirical standard deviation $sd(Y_t')$ of $Y_t'(s) = \sqrt{Y_t(s)}$: amplitude trends with respect event magnitude typically lead to trends in this summary value; the square root transformation ensures finite standard deviation values.

Several empirical studies on climate data show that extremal dependence may weaken when the event magnitude increases (Opitz et al., 2015; Huser and Wadsworth, 2018; Le et al., 2018; Tawn et al., 2018). Then, asymptotic independence may ultimately arise, or the dependence strength may stabilize at very high but unobserved magnitudes. We cannot check this stability behavior with absolute certainty in finite samples. If the extremal dependence strength continues to weaken in data above the selected threshold u, we acknowledge that our GP process framework leads to rather conservative probability estimates for observing concomitant high values.

4. Methodology for uplifting observed extreme episodes

We now describe the general procedure for the extraction of extreme space-time episodes (Section 4.1) and the algorithm to resample new space-time scenarios (Section 4.2). A probabilistic interpretation of such resampling is given in Section 4.3. Throughout and without loss of generality, we here use the same notation for the single observation of the space-time process $X(s,t)$ and the stochastic process itself.

4.1. Selection of extreme episodes

Algorithm 1 describes the extraction of extreme episodes from standardized data X^*. To start, we define the space-time neighborhoods $\mathcal{N}(s,t)$ scanned for extreme episodes by applying the cost functional ℓ, whose values represent the event magnitude. If ℓ is applied to the full study region, we may drop the index s and simply write $\mathcal{N}(t)$. We choose a threshold u for the cost functional above which the asymptotic stability properties underpinning our approach are (approximately) satisfied. There must be at least one exceedance of the cost functional above the threshold in the data set. The first step of the algorithm is to compute the values of ℓ for each neighborhood $\mathcal{N}(s,t)$. We select as the first extreme episode the neighborhood $\mathcal{N}(s_1,t_1)$ where $\ell_{s,t}$ reaches its maximum value ℓ_1. We aim at extracting a collection of extreme episodes that are at most weakly dependent; therefore, the algorithm needs a mechanism to "decluster" extreme episodes. The second extracted extreme episode corresponds to the maximum value of

$\ell_{s,t}(X^*)$ arising in the data set $X^*(s,t)$ with t in the set of reduced time steps after removal of time steps that intersect with $\mathcal{N}(s_1,t_1)$ or, more generally, with a larger temporal buffer zone $\mathcal{N}_{\text{buffer}}(t_1)$ around t_1. We then iterate this procedure of episode extraction and data set reduction. The stopping criterion for the extraction of extreme episodes is two-fold: either a fixed target number m' of extreme episodes is reached, or the extreme condition $\ell_{s,t}(X^*) > u$ for a fixed high threshold u cannot be fulfilled any longer in the reduced data set.

4.2. Semi-parametric simulation method

To sample new extreme space-time scenarios, we proceed as follows:

(a) **Standardization**: Estimate marginal tail parameter functions $\gamma(s,t)$, $\sigma(s,t)$ and $\mu(s,t)$ in (6), and denote by $X^* = \{T(X(s,t))\}_{s\in\mathcal{S},t\in\mathcal{T}}$ the resulting standardized process (5).

(b) **Selection of extreme episodes**: Fix the maximum number of extreme episodes m'. Use Algorithm 1 to extract the collection of $m \le m'$ extreme episodes $X^*_{[i]}$, $i = 1,\dots,m$.

(c) **Lifting**: Sample R_i, $i = 1,\dots,m'$ according to a Pareto distribution with shape 1 and scale $\alpha > 0$, i.e. $\mathbb{P}(R_i > x) = \alpha/x$, $x \in [\alpha,\infty)$, and generate lifted extreme episodes as

$$V_i(s,t) = R_i \frac{X^*_{[i]}(s,t)}{\ell_i} = R_i Y_i(s,t),\ (s,t) \in \mathcal{N}(s_i,t_i). \tag{10}$$

(d) **Back-transformation to original scale**: Lifted extreme episodes are transformed back to the original marginal scale by $W_i(s,t) = T^{\leftarrow}(V_i(s,t))$, $(s,t) \in \mathcal{N}(s_i,t_i)$.

4.3. Interpretation of our proposed model

According to Definition 2, the lifting procedure in Section 4.2 samples new realizations V_i of a space-time Pareto process with support $\mathcal{N}(s_i,t_i)$ for each extreme episode i. Since $\mathbb{P}(\ell(X^*) > x) \sim \theta_\ell/x$ for large x and since resampled scale variables R_i are larger than α, we obtain α/θ_ℓ as the minimum return period for resampled extreme episodes. Moreover, choosing a larger α will generate resampled extreme episodes with longer return period.

We can further establish a link between our resampling procedure and the linear normalization constants in (3) leading to a max-stable limit at the original marginal scale. A valid choice for b_n, as suggested by EVT, is the $(1-1/n)$-quantile of $F_{(s,t)}$. With resampled scaling variable $R_i = r_i$ and the originally observed one ℓ_i (see Sections 4.1-4.2), and with appropriately chosen events A, we can follow arguments similar to Chailan et al. (2017, Appendix) and show that

$$P\left(\frac{W_i(s,t)-b_{nc}}{a_{nc}} \in A \middle| R_i = r_i, \ell_{s,t}(X^*) = \ell_i\right) \approx P\left(\frac{X_{[i]}(s,t)-b_n}{a_n} \in A \middle| R_i = r_i, \ell_{s,t}(X^*) = \ell_i\right),$$

Algorithm 1: Algorithm for selecting extreme episodes defined over space-time neighborhoods $\mathcal{N}(s,t)$. In Step 8, instead of extracting only the extreme neighborhood $\mathcal{N}(s_i,t_i)$, we may sometimes want to extract the full study domain $\mathcal{N}(t_i)\times\mathcal{S}$.

Input:

- $\{X^*(s,t), s\in\mathcal{S}, t\in\mathcal{T}\}$, space-time observations on a standardized scale;
- $\mathcal{S}'\subseteq\mathcal{S}$ sites of interest and $\mathcal{T}'\subseteq\mathcal{T}$ time steps of interest.
- m' the maximum number of extreme episodes to select;
- u threshold on $\ell_{s,t}(X^*)$ for the selection of extreme episodes;
- $\delta=\delta_1+\delta_2+1$ with $\delta_1,\delta_2\geq 0$ the duration of extreme episodes defining temporal neighborhoods $\mathcal{N}(t)=[t-\delta_1,t+\delta_2]$;
- $\beta_1,\beta_2\geq 0$ buffer time steps to ensure independent extreme episodes defining extended temporal neighborhoods $\mathcal{N}_{\text{buffer}}(t)=[t-\delta_1-\beta_1,t+\delta_2+\beta_2]$;
- $\mathcal{N}(s)$ spatial neighborhood for $s\in\mathcal{S}'$, such that $\mathcal{N}(s,t)=\mathcal{N}(s)\times\mathcal{N}(t)$.

Output:

- m: the number of selected extreme episodes ($m\leq m'$);
- $\left\{X^*_{[1]},X^*_{[2]},\ldots,X^*_{[m]}\right\}$, $\{s_1,t_2,\ldots,s_m\}$, $\{t_1,t_2,\ldots,t_m\}$, $\{\ell_1,\ell_2,\ldots,\ell_m\}$: collection of extreme episodes; observation sites and times; aggregation values related to extreme episodes.

1 **begin**
2 Set $\mathcal{I}=\mathcal{T}'$.
3 Calculate $\ell_{s,t}(X^*)$ for all $t\in\mathcal{T}', s\in\mathcal{S}'$ with $\mathcal{N}(s,t)\subset\mathcal{S}\times\mathcal{T}$.
4 $i\leftarrow 1$.
5 **while** $i\leq m'$ *and* $\max_{s\in\mathcal{S}',t\in\mathcal{I}}\ell_{s,t}(X^*)>u$ **do**
6 $(s_i,t_i)\leftarrow\arg\max_{t\in\mathcal{I},s\in\mathcal{S}'}\ell_{s,t}(X^*)$
7 $\ell_i\leftarrow\ell_{s_i,t_i}(X^*)$
8 $X^*_{[i]}\leftarrow\{X^*(s',t'),\ (s',t')\in\mathcal{N}(s_i,t_i)\}$
9 $\mathcal{I}\leftarrow\mathcal{I}\setminus\mathcal{N}_{\text{buffer}}(t_i)$
10 $i=i+1$
11 **return** m, $\left\{X^*_{[1]},X^*_{[2]},\ldots,X^*_{[m]}\right\}$, $\{s_1,s_2,\ldots,s_m\}$, $\{\ t_1,t_2,\ldots,t_m\}$, $\{\ell_1,\ell_2,\ldots,\ell_m\}$

as $n \to \infty$, where $c = r_i/(\ell_i \theta_\ell)$. Therefore, the resampled and backtransformed episode $W_i(s,t)$ has approximately the same probability distribution as the observed extreme episodes in $X(s,t)$, except for b_n and a_n replaced by b_{nc} and a_{nc}. If $\alpha > \theta_\ell \ell_i$, then $b_{nc} > b_n$, and our procedure generates a threshold-stable stochastic process at a higher level than the observed one.

5. Application to precipitation in Mediterranean France

We use our resampling algorithm to produce large numbers of realistic spatio-temporal extreme precipitation scenarios in a region in Mediterranean France where flash floods are frequent, and we show how to calculate two risk measures for the most extreme observed space-time episodes before and after uplifting them to longer return periods.

5.1. Description of the data set

Our semi-parametric approach does not provide for a mechanism to spatially interpolate observations; therefore, precipitation measurements should be available over a sufficiently dense network of sites. We here use hourly precipitation reanalysis data over a 1 km^2 grid, constructed by merging radar signals and observed hourly precipitation totals (Tabary et al., 2012). The grid has $10,914$ cells covering a 133.2 km $\times$ 104.3 km area in Mediterranean France, see Figure 1, with $87,642$ hourly time steps covering the 10-year period from 1997 to 2007. The unit of measurement is mm/h. This data set was provided by *Météo-France* (http://www.meteofrance.com). The large dimension of the data set allows us to disregard restrictive parametric assumptions in favour of a nonparametric approach for the extremal dependence model.

Empirical return levels of rainfall intensities at the 98% level (i.e., of strictly positive observations) and the maximum precipitation values observed over the complete study period are reported for each grid cell in Figure 1.

5.2. Standardisation of marginal distributions

The first step of our lifting procedure is the definition of a marginal transformation T, appropriate for extreme hourly precipitation data, to obtain the standardized process X^* in (5). We first discuss our choice of the target distribution G. Due to the hourly temporal resolution, values 0 occur with very high frequency in the data. Therefore, we include a discrete mass p_0 at 0 to represent absence of precipitation. Following Opitz (2016), we construct G to have mass $p_0 \geq 0$ at 0, a uniform density on $(0, x_0)$, and a standard Pareto distribution for $x > x_0$ where $x_0 > 1$.

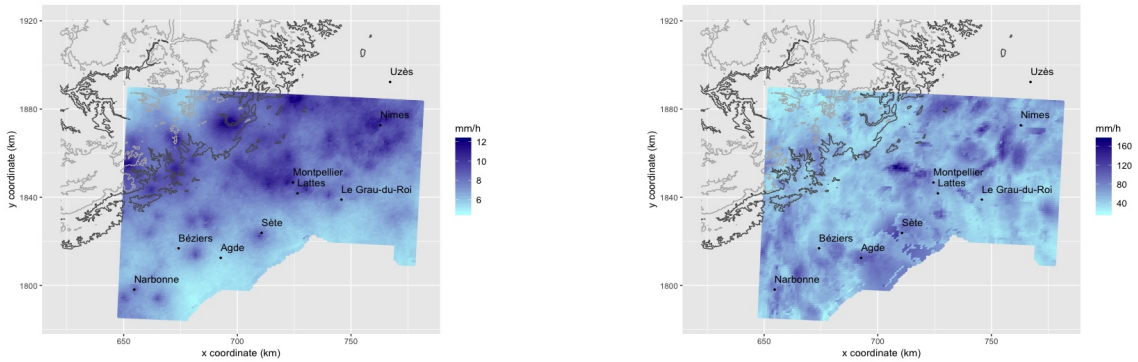

Fig. 1. Empirical return levels at 98% level (left panel) and maxima (right panel) of hourly precipitation intensities for each grid cell in our study area from 1997 to 2007.

The junction point x_0 is chosen to ensure continuity of the density of G for $x > 0$:

$$G(x) = \begin{cases} 0, & x < 0, \\ p_0, & x = 0, \\ p_0 + \frac{(1-p_0)^2}{4}x, & 0 < x \leq 2/(1-p_0), \\ 1 - 1/x, & x > 2/(1-p_0). \end{cases} \tag{11}$$

An illustration of G for $p_0 = 0.7$ is provided in Figure 2 in the supplementary material. Next, we choose the distribution function $F_{(s,t)}$ of $X(s,t)$ as the empirical distribution function $F_{(s)}$ (i.e., at each grid cell s) when $X(s,t) \leq u(s,t)$, and according to (6) when $X(s,t) > u(s,t)$. We use spatial models for the marginal tail parameters, whose estimators $\hat{\mu}(s)$, $\hat{\sigma}(s)$ and $\hat{\gamma}(s)$ in $F_{(s)}$ are obtained by composite marginal likelihood inference (Varin et al., 2011) using a threshold $u(s)$ chosen as a high empirical quantile for fixed s; here, we choose the 0.95-quantile of hourly rainfall intensities. Thanks to the consistency of these estimators and the continuity of T, we can apply the continuous mapping theorem such that the transformation $\hat{T}$ (with estimators plugged in) is a consistent estimate of T.

5.3. Choice of spatio-temporal cost functionals

Our first cost functional $\ell^{(1)}_{s,t}$ is a *spatio-temporal average*, i.e., the average value of $X^*(s,t)$ over the spatio-temporal neighborhoods $\mathcal{N}(s,t)$, for all feasible space-time points (s,t). In space, we specify this neighborhood through a 15 km disc centered at s; in time, it extends backward from t such that $\mathcal{N}(t) = \{t-\delta+1, \ldots, t\}$ with duration $\delta = 12$ hours. With this choice, $\theta_{\ell^{(1)}_{s,t}} = 1$, see Sections 3.2 and 4.3. The second cost functional $\ell^{(2)}_t$ is in line with classical spatial EVT and is called *spatial maximum*; the value $\ell^{(2)}_t(X^*)$ corresponds to the maximum over the whole

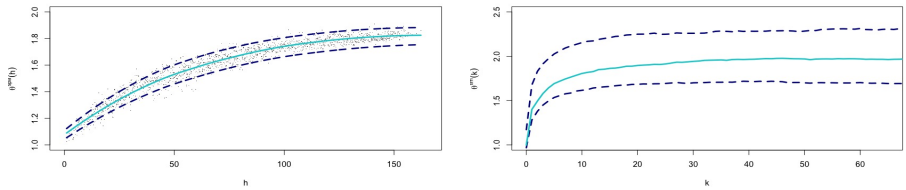

Fig. 2. Extremal coefficient functions. Left: $\hat{\theta}^{spa}(h)$, based on a subsample of 1500 pairs of grid cells, with a local polynomial regression (turquoise line). Right: $\hat{\theta}^{tim}(k)$, based on pairs of spatial maxima separated by a time lag k (turquoise line). Dashed lines show bootstrap confidence intervals at 95%.

study area at hour t. For this choice, we need an estimate of the extremal coefficient $\theta_{\ell_t^{(2)}}$ to obtain return levels for lifted events. Therefore, we implement maximum censored likelihood for estimating the scale parameter $\theta_{\ell_t^{(2)}}$ of a Pareto distribution with fixed shape 1, using observed magnitudes $\ell_t^{(2)}(X^*)$ censored below a high threshold u.

5.4. Analysis of extremal dependence properties

Using techniques proposed in Section 3.3, we first illustrate pairwise empirical extremal coefficients with respect to spatial distance and temporal lags, and we then check if threshold stability is a valid assumption for the data set when considering high quantiles.

Figure 2 shows the estimations of the empirical spatial and temporal extremal coefficient functions. The pairwise estimator is based on a threshold for each of the two components, see Section 3 of the supplementary material for details. The empirical spatial extremal coefficient function is plotted in Figure 2 (left panel). For θ^{spa}, the threshold $u(s)$ is set to the empirical 0.98-quantile of $X^*(s,\cdot)$ where s represents the site with maximum empirical 0.98-quantile between the two sites involved the pairwise estimator. The empirical temporal extremal coefficient function is plotted in Figure 2 (right panel). In this case, a uniform threshold u is chosen as the empirical 0.98-quantiles of the sample of spatial maxima $\ell_t^{(2)}(X^*)$. Pointwise block bootstrap confidence intervals at 95% for both extremal coefficient function are constructed using variable size blocks with block length following a geometric distribution with mean 300 hours (Politis and Romano, 1994; Davis et al., 2011). Figure 2 shows that $\hat{\theta}^{spa}(h)$ and $\hat{\theta}^{tim}(k)$ are always below 2, hinting at substantial extremal dependence at finite, observed quantile levels. We see that the maximum duration of extreme episodes is approximately 12 hours. We point out that there is a certain sensitivity of the estimated curves with respect to the probability p used for fixing empirical thresholds u, with a slight tendency towards decreasing dependence strength at

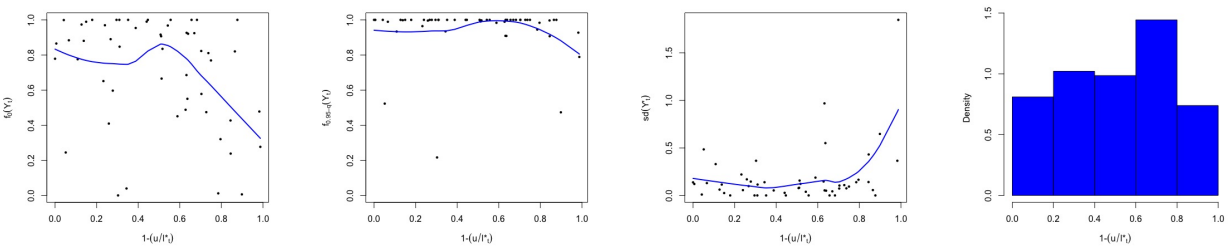

Fig. 3. Analysis of scale-profile independence for the spatio-temporal average. The threshold u is chosen as the 0.95-quantile of observed magnitudes $\ell_t^{(1)}(X^*)$. From left to right: $f_{u'}(Y_i)$ for $u' = 0$; same for $u' = 0.95$-quantile; $\mathrm{sd}(Y_i')$; histogram of $1 - u/\ell_i^*$.

higher levels; see Figure 1 in the supplementary material.

Next, we complement these findings by checking spatial threshold stability based on the independence of scales and profiles for high event magnitudes observed at a given time. First, we point out that certain calculations for extreme episodes were quite sensitive to the high proportion of 0 values (i.e., absence of precipitation) in the data set, which amount to around 92 %. Therefore, we add a preprocessing step where we remove hourly time steps t_i from the data set if the precipitation totals in a sliding 24hour-window centered at t_i, cumulated over all grid cells, are smaller than 550 mm, corresponding to a spatially averaged precipitation total of 0.05 mm over 24 hours. The resulting data subset retained contains only around 23 % of 0 values. Now, we check the scale-profile independence for the case of the spatio-temporal average $\ell_{s,t}^{(1)}$, and for simplicity we here consider the full study area $\mathcal{S}$ as spatial support, and we write $\ell_t^{(1)}$ for the resulting cost functional. The empirical 0.95-quantile of $\ell_t^{(1)}(X^*)$ is used as threshold u. Denote by $Y_i = \{Y_i(s,t)\}$ the observed profile process Y_t corresponding to each extracted extreme episode i, with $i = 1, \ldots, m$. In the two displays on the left of Figure 3, the proportion of profile process values $Y_i(s,t)$ below or equal to a threshold $u' \geq 0$, denoted by $f_{u'}(Y_i)$, is plotted for $u' = 0$ and for u' fixed to the empirical 0.95-quantile of all episodes Y_i taken together. The empirical standard deviation $sd(Y_i')$ of the square root $Y_i'(s,t)$ of profile process values $Y_i(s,t)$ is depicted in the third display of Figure 3. For easier visual interpretation, both summary statistics are plotted against $1 - u/\ell_i^*$, where $\ell_i^* = \ell_{t_i}^{(1)}(X_{[i]}^*)$. Under the functional domain-of-attraction assumption, the distribution of $1 - u/\ell_i^*$ is approximately uniform on $[0,1]$. Histograms of $1 - u/\ell_i^*$ are shown in the fourth display of Figure 3, and no striking deviation from uniformity appears. Moreover, it is difficult to detect strong systematic trends in profile values with respect to event magnitude. Judging from the shape of the local regression curves

in this plot, e.g. for $sd(Y_i')$, we may be in a border case between asymptotic dependence and asymptotic independence, but it is difficult to decide with certitude. If date do not satisfy asymptotic dependence, we acknowledge that our resampling procedure may lead to rather conservative estimates aggregated extreme risks. In the following, we assume that domain-of-attraction properties are satisfied for our data set if we fix the 0.95-quantile as threshold for $\ell_{s,t}^{(1)}(X^*)$ given as the spatio-temporal average function. Similar conclusions are valid for the spatial maximum $\ell_t^{(2)}$ with u given as the 0.98-quantile.

5.5. Parameter choice for extreme episode extraction and lifting

As before with $\ell_{s,t}^{(1)}$, we fix the duration of extreme episodes to 12 hours (i.e., $\delta = 12$ in Algorithm 1). The sliding temporal neighborhood $\mathcal{N}(t)$ of extreme episodes is defined differently for $\ell_{s,t}^{(1)}$ and $\ell_t^{(2)}$. While the time step t_i (where the maximum of the cost functional occurs for the ith extreme episode) is placed at the end of the time window for the spatio-temporal average (i.e., $\delta_1 = 11$ and $\delta_2 = 0$ in Algorithm 1), t_i is set in the middle of the time window for the spatial maximum (i.e., $\delta_1 = 5$ and $\delta_2 = 6$ in Algorithm 1). Furthermore, the spatial neighborhoods $\mathcal{S}'$ are chosen differently for the two ℓ functions. In order to calculate $\ell_{s,t}^{(1)}$, we consider a spatial neighborhood of 15 kms around each reference point s, such that $\mathcal{S}'$ is composed of sites s with minimum distance of 15 km to the boundary of the study region. However, for $\ell_{s,t}^{(1)}$, in Step 8 in Algorithm 1, we extract the full study domain. For $\ell_t^{(2)}$, we always take $\mathcal{S}' = \mathcal{S}$. To generate independent extreme episodes, we remove δ_1 time steps before t_i (i.e., $\beta_1 = 0$) and $\beta_2 = 12$ after t_i for the spatio-temporal average; and, we take $\beta_1 = \beta_2 = 6$ for the spatial maximum. In order to illustrate a strong uplifting effect in resampled extreme episodes, we select a high lower threshold for newly sampled scale variables R_i, i.e. a large scale parameter α for Pareto distribution with shape 1, here given by twice the maximum value of observed magnitudes $\ell_i^{(1)}(X^*)$ and $\ell_i^{(2)}(X^*)$. In general, the parameter choice in our method provides high flexibility with respect to the modeling context.

5.6. Spatio-temporal extreme precipitation scenarios

We report the starting time $t_i - 11$ for the 6 most extreme precipitation episodes with respect to the spatio-temporal average $\ell_{s,t}^{(1)}$ in the second column of Table 1. Analogously, for the spatial maximum functional $\ell_t^{(2)}$ the starting times $t_i - 5$ are presented in the third column Table 1.

In general, we remark that both cost functionals extract similar extreme episodes in terms of temporal neighborhoods, but the order with respect to event magnitudes is different. Some

Table 1. Starting times of the most extreme, temporally declustered space-time episodes extracted by considering two different cost functionals.

Episode	**Spatio-temporal average** $\ell_{s,t}^{(1)}$	**Spatial maximum** $\ell_t^{(2)}$
1st	2005-09-06 12:00:00	2005-09-06 14:00:00
2nd	1999-09-03 07:00:00	1999-09-13 23:00:00
3rd	2006-10-11 13:00:00	1999-08-28 11:00:00
4th	2002-09-08 11:00:00	1999-09-03 04:00:00
5th	1999-10-17 20:00:00	2001-07-05 18:00:00
6th	2001-07-05 15:00:00	2006-10-11 15:00:00

extreme episodes arise only for one of the two cost functionals.

Figure 4 shows the original precipitation data $X(s,t)$ and the final uplifted scenarios $W(s,t)$ for several time steps from the extracted temporal neighborhoods for the spatio-temporal average $\ell_{s,t}^{(1)}$. We see a clear increase in intensity in the uplifted precipitation fields in Figure 4. Analog plots for $\ell_t^{(2)}$ are presented in in the supplementary material (Figure 3).

5.7. Risk analysis

The two risk measures applied in the following are detailed in Section 2 of the supplementary material. We perform a risk analysis that aims at exploring differences in uplifted extreme episodes that can be imputed to the choice of cost functionals and of the fixed lower threshold (i.e., the Pareto scale parameter) used for sampling new scale variables R_i. We consider the 3 largest episodes extracted for each of the two cost functionals $\ell_{s,t}^{(1)}$ and $\ell_t^{(2)}$, see Table 1. We uplift these episodes using R_i as the 0.25-, 0.5- and 0.75- quantiles of the Pareto random distribution with shape 1 and scale α_i, $i = 1, \ldots, 4$ with α_1 corresponding to the value of the cost functional for the most extreme episode centered at t_1, and then $\alpha_2 = 2\alpha_1$, $\alpha_3 = 3\alpha_1$ and $\alpha_4 = 4\alpha_1$.

Two univariate risk measures – the quantile for a fixed probability (*return level*), and the Conditional Tail Expectation (CTE) – are computed for the original episode and for each uplifted episode W_i, where we first aggregate values of $X(s,t)$ and $W(s,t)$ respectively for each spatial grid cell by taking its temporal average over the 12 time steps. Figure 5 presents quantiles at the two levels 0.98 and 0.99 according to the two cost functionals and with the four lower thresholds α_i for the Pareto-distributed scaling variable. Along the ordinate axes, we also report the quantiles for each of the three original episodes. Clearly, Figure 5 shows the higher α leads to higher risk. Furthermore, for both cost functionals we see that the highest risk is attributed to the episode with highest magnitude, the first extreme episode (see Figure 5).

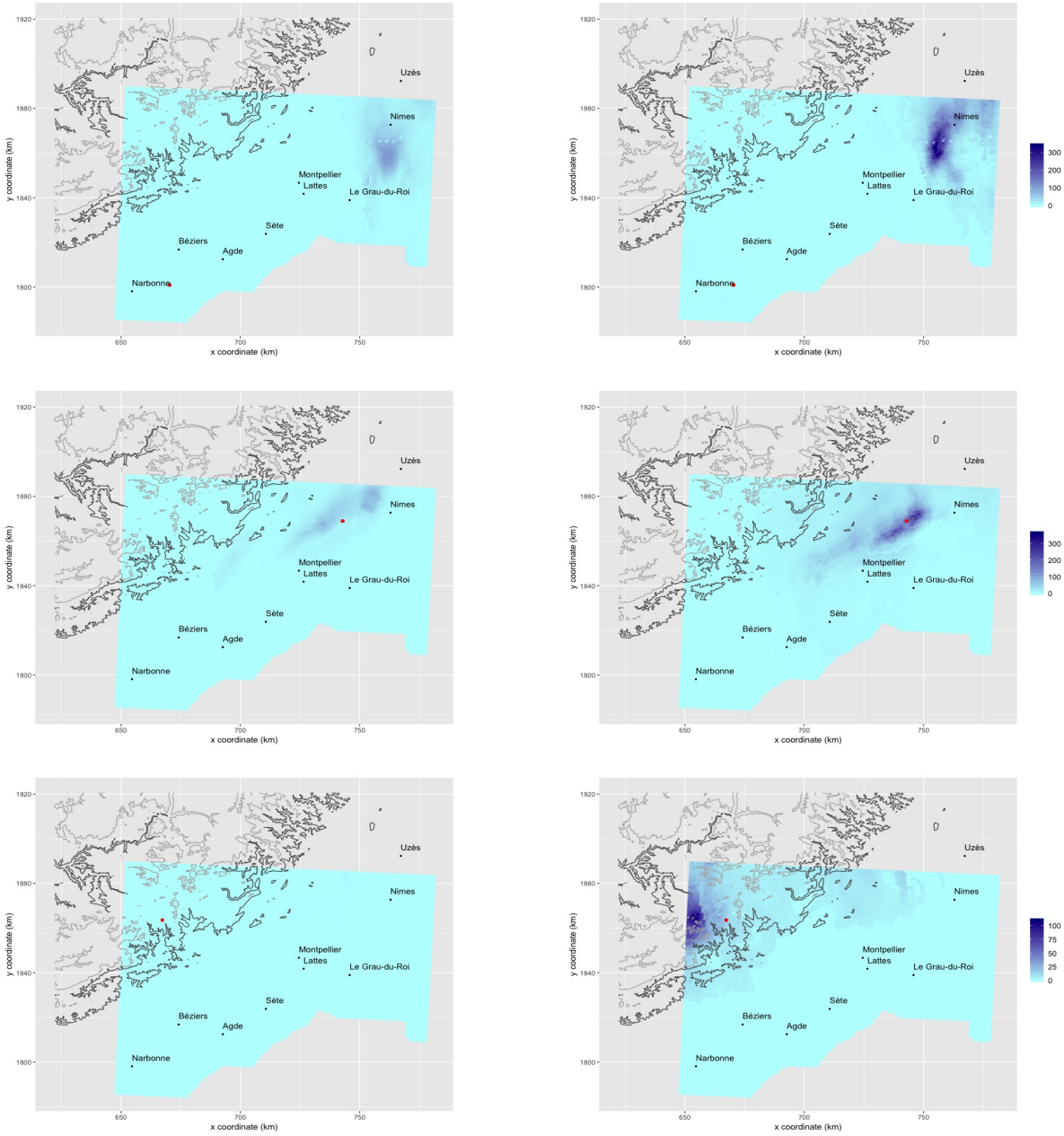

Fig. 4. Original precipitation data $X(s,t)$ (left column) and uplifted episodes $W(s,t)$ (right column) based on the spatio-temporal average $\ell^{(1)}_{s,t}$. First row: extreme episode associated to t_1, here shown for t =2005-09-06, 14:00:00; second row: same for t_4 and t =2002-09-08, 15:00:00; third row: same for t_6 and t =2001-07-06, 00:00:00. The red dots indicate the site s_i where the maximum value $\ell^{(1)}_{s_i,t_i}$ as been observed during the episode.

However, the third-highest magnitude event yields higher risk than the second-highest one, as can be seen for the spatial maximum cost functional (see right column of Figure 5). Indeed, the spatial maximum ℓ may tend to select episodes with highly localized peaks, i.e. there may be a large majority of zeros or small values with a few spatially confined clusters of very large precipitation intensities. On the other hand, risk measures based on spatio-temporal averages better account for the persistence of moderate to high precipitation intensities. These contrasted results highlight that many ways exist to order elements (here: space-time episodes) defined over high-dimensional spaces (here: space-time neighborhoods $\mathcal{N}(s,t)$); we underline that the mechanism of cost functionals allows the user to make a flexible choice that is appropriate in the modeling context. In addition, in the case of $\ell_{s,t}^{(1)}$, we expect uplifted episodes with the same return periods since $\theta_\ell = 1$ and we use the same realization R (see Section 4.3). Therefore, we obtain greater return levels when the extremeness increases. Similar conclusions are obtained for the CTE risk measure, see Figure 4 in the supplementary material.

6. Conclusion and outlook

In this work, we set up a general framework for space-time generalized Pareto process. It allowed us to develop a semi-parametric method to simulate extreme space-time scenarios of phenomenona such as precipitation. The extremal dependence structure is fully data-driven, and we require parametric assumptions only for the univariate tails, based on EVT. A crucial component is the cost functional defined over a sliding space-time window. It characterizes extreme episodes as episodes whose "cost" exceeds a high threshold. The application of our method to a gridded precipitation data set in Mediterranean France was used for a relatively simple risk analysis. It illustrates how cost functionals can be defined, how these affect the selection of extreme episodes, and how the magnitude of the newly sampled scale variables impacts the magnitude of the lifted extreme episodes on the original marginal scale.

In future work, space-time distance metrics other than the Euclidean distance could be used to define the space-time neighborhoods $\mathcal{N}(s,t)$. To account for orographic structures, the crossing distance could be used, which includes a vertical component related to the crossing of crests and valleys (Gottardi et al., 2012). Instead of fitting the marginal tail parameters separately for each grid cell, a generalized additive regression approach could be implemented to borrow information from nearby sites (Gardes and Girard, 2010; Carreau et al., 2017). Finally, by extending ideas in Yiou (2014), we plan to implement our method as part of a spatial precipitation generator that simulates complete rainfall series including dry, ordinary and extreme events. Precipitation

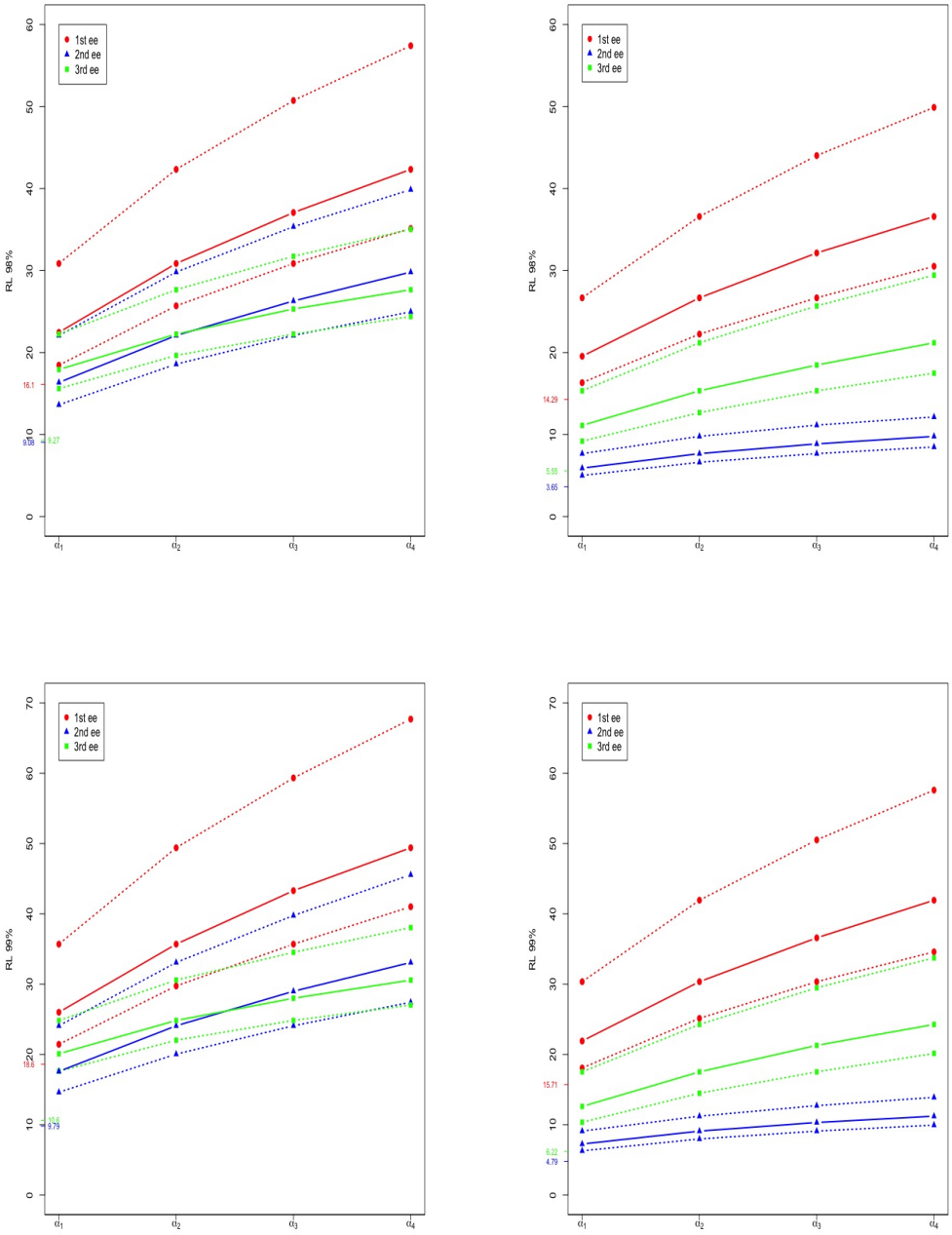

Fig. 5. Return level at 98% (first row) and at 99% (second row). Left: spatio-temporal average cost function. Right: spatial maximum cost functional. The legend indicates the extreme episode (ee). For each episode, the lines correspond to different uplifting levels using the 0.25-, 0.5- and 0.75- quantile (from bottom to top) of the Pareto distribution of the scaling variable with shape 1 and scale α_i, $i = 1, \ldots, 4$.

generator output will then by fed to rain-flow models to conduct impact studies.

References

Beirlant, J., Goegebeur, Y., Segers, J. and Teugels, J. (2004) *Statistics of Extremes: Theory and Applications.* Wiley Series in Probability and Statistics.

Caires, S., de Haan, L. and Smith, R. L. (2011) On the determination of the temporal and spatial evolution of extreme events. *Deltares report 1202120-001-HYE-004 (for Rijkswaterstaat, Centre for Water Management).*

Carreau, J., Naveau, P. and Neppel, L. (2017) Partitioning into hazard subregions for regional peaks-over-threshold modeling of heavy precipitation. *Wat. Resour. Res*, **53(5)**, 4407–4426.

Chailan, R., Toulemonde, G. and Bacro, J. N. (2017) A semiparametric method to simulate bivariate space-time extremes. *Ann. Appl. Statist.*, **11(3)**, 1403–1428.

Coles, S. (2001) *An Introduction to Statistical Modeling of Extreme Values.* Springer Series in Statistics.

Davis, R. A., Klüppelberg, C. and Steinkohl, C. (2013a) Max-stable processes for modeling extremes observed in space and time. *J. Korean Statist. Soc.*, **42(3)**, 399–414.

— (2013b) Statistical inference for max-stable processes in space and time. *J. R. Statist. Soc. B*, **75(5)**, 791–819.

Davis, R. A., Mikosch, T. and Cribben, I. (2011) Estimating Extremal Dependence in Univariate and Multivariate Time Series via the Extremogram. *arxiv:1107.5592v1.*

Dombry, C., Engelke, S. and Oesting, M. (2016) Exact simulation of max-stable processes. *Biometrika*, **103(2)**, 303–317.

Dombry, C., Eyi-Minko, F. and Ribatet, M. (2013) Conditional simulation of max-stable processes. *Biometrika*, **100**, 111–124.

Dombry, C. and Ribatet, M. (2015) Functional regular variations, Pareto processes and peaks over threshold. *Statistics and Its Interface*, **8(1)**, 9–17.

Embrechts, P., Klüppelberg, C. and Mikosch, T. (1997) *Modelling extremal events for insurance and finance.* Springer. Berlin.

Engelke, S., de Fondeville, R. and Oesting, M. (2018) Extremal behaviour of aggregated data with an application to downscaling. *Biometrika: https://doi.org/10.1093/biomet/asy052.*

European Environment Agency (2007) Directive 2007/60/ec of the European parliament and of the council of 23 October 2007 on the assessment and management of flood risks. OJ L. 288: 27-34.

Ferreira, A. and de Haan, L. (2014) The generalized Pareto process; with a view towards application and simulation. *Bernoulli*, **20(4)**, 1717–1737.

— (2015) On the block maxima method in extreme value theory: PWM estimators. *Ann. Statist.*, **43(1)**, 276–298.

Ferreira, A., de Haan, L. and Zhou, C. (2012) Exceedance probability of the integral of a stochastic process. *J. Multiv. Anal.*, **105(1)**, 241–257.

French, J., Kokoszka, P., Stoev, S. and Hall, L. (2018) Quantifying the risk of heat waves using extreme value theory and spatio-temporal functional data. *Computnl Statist. Data Anal.*, **131**, 176–193.

Gardes, L. and Girard, S. (2010) Conditional extremes from heavy-tailed distributions: an application to the estimation of extreme rainfall return levels. *Extremes*, **13(2)**, 177–204.

Gottardi, F., Obled, C., Gailhard, J. and Paquet, E. (2012) Statistical reanalysis of precipitation fields based on ground network data and weather patterns: Application over French mountains. *Journal of Hydrology*, **432-433**, 154–167.

de Haan, L. (1984) A spectral representation for max-stable processes. *Ann. Probab*, **12(4)**, 1194–1204.

de Haan, L. and Ferreira, A. (2006) *Extreme Value Theory. An Introduction.* Springer Series in Operations Research and Financial Engineering. Springer: New York.

Huser, R. and Wadsworth, J. L. (2018) Modeling spatial processes with unknown extremal dependence class. *J. Am. Statist. Ass., DOI: 10.1080/01621459.2017.1411813.*

Le, P. D., Davison, A. C., Engelke, S., Leonard, M. and Westra, S. (2018) Dependence properties of spatial rainfall extremes and areal reduction factors. *Journal of Hydrology*, **565**, 711–719.

Lin, T. and de Haan, L. (2001) On convergence toward an extreme value distribution in c[0,1]. *Ann. Probab*, **29(1)**, 467–483.

McPhillips, L. E., Chang, H., Chester, M. V., Depietri, Y., Friedman, E., Grimm, N. B., Kominoski, J. S., McPhearson, T., Méndez-Lázaro, P., Rosi, E. J. and Shafiei Shiva, J. (2018) Defining extreme events: A cross-disciplinary review. *Earth's Future*, **6**, 441–455.

Oesting, M., Bel, L. and Lantuéjoul, C. (2018a) Sampling from a max-stable process conditional on a homogeneous functional with an application for downscaling climate data. *Scand. J. Statist.*, **45(2)**, 382–404.

Oesting, M., Schlather, M. and Zhou, C. (2018b) Exact and fast simulation of max-stable processes on a compact set using the normalized spectral representation. *Bernoulli*, **24(2)**, 1497–1530.

Opitz, T. (2016) Modeling asymptotically independent spatial extremes based on laplace random fields. *Spatial Statistics*, **16**, 1–18.

Opitz, T., Bacro, J. N. and Ribereau, P. (2015) The spectrogram: A threshold-based inferential tool for extremes of stochastic processes. *Electron. J. Stat.*, **9**, 842–868.

Pickands III, J. (1975) Statistical inference using extreme order statistics. *Ann. Statist.*, **3**, 119–131.

Politis, D. N. and Romano, J. P. (1994) The stationary bootstrap. *J. Am. Statist. Ass.*, **89**, 1303–1313.

Rootzén, H. and Tajvidi, N. (2006) Multivariate generalized pareto distributions. *Bernouilli*, **12(5)**, 917–930.

Tabary, P., Dupuy, P., LHenaff, G., Gueguen, C., Moulin, L., Laurantin, O., Merlier, C. and Soubeyroux, J.-M. (2012) A 10-year (1997–2006) reanalysis of quantitative precipitation estimation over france: methodology and first results. *IAHS Publ*, **351**, 255–260.

Tawn, J., Shooter, R., Towe, R. and Lamb, R. (2018) Modelling spatial extreme events with environmental applications. *Spatial Statistics, DOI:10.1016/j.spasta.2018.04.007.*

Thibaud, E. and Opitz, T. (2015) Efficient inference and simulation for elliptical Pareto processes. *Biometrika*, **102(4)**, 855–870.

Varin, C., Reid, N. and Firth, D. (2011) An overview of composite likelihood methods. *Statistica Sinica*, **21(1)**, 5–42.

Vinet, F., Boissier, L. and Saint-Martin, C. (2016) Flash flood-related mortality in southern France: first results from a new database. *E3S Web of Conferences 7, article number 06001*, **3**, 3397–3438.

Yiou, P. (2014) Anawege: a weather generator based on analogues of atmospheric circulation. *Geoscientific Model Development*, **7**, 531–543.